Published in final edited form as:
Neuron. 2009 February 26; 61(4): 609–620. doi:10.1016/j.neuron.2009.01.006.

Synapses with inhibitory neurons differentiate anterior cingulate from dorsolateral prefrontal pathways associated with cognitive control

M. Medalla[1] and **H. Barbas**[1,2]

[1] Department of Health Sciences, Boston University and School of Medicine, Boston, MA

[2] Program in Neuroscience, Boston University and School of Medicine, Boston, MA

Summary

The primate dorsolateral prefrontal cortex (DLPFC) and anterior cingulate cortex (ACC) focus attention on relevant signals and suppress noise in cognitive tasks. However, their synaptic interactions and unique roles in cognitive control are unknown. We report that two distinct pathways to DLPFC area 9, one from the neighboring area 46 and the other from the functionally distinct ACC, similarly innervate excitatory neurons associated with selecting relevant stimuli. However, ACC has more prevalent and larger synapses with inhibitory neurons and preferentially innervates calbindin inhibitory neurons, which reduce noise by inhibiting excitatory neurons. In contrast, area 46 mostly innervates calretinin inhibitory neurons, which disinhibit excitatory neurons. These synaptic specializations suggest that ACC has a greater impact in reducing noise in dorsolateral areas during challenging cognitive tasks involving conflict, error, or reversing decisions, mechanisms that are disrupted in schizophrenia. These observations highlight the unique roles of the DLPFC and ACC in cognitive control.

Keywords

Macaca mulatta; anterior cingulate; dorsolateral prefrontal; calbindin; calretinin; parvalbumin; inhibitory neurons

Introduction

The ability to keep track of information and one's actions from moment to moment is necessary to accomplish even the simple tasks of everyday life. Lateral prefrontal cortices in primates, especially dorsolateral areas 46 and 9, have a key role in the process broadly called working memory (Goldman-Rakic, 1995; Tanji and Hoshi, 2008). Lesions of areas 46 and 9 show similar and cumulative deficits in monitoring the sequence of information in working memory tasks (Petrides, 2000; Muller and Knight, 2006). The ACC is involved in affective and mnemonic processing, but is also engaged in cognitive operations, especially in tasks with high

Please address correspondence: Helen Barbas, Dept. Health Sciences, Boston University, 635 Commonwealth Ave. Room 431, Boston, MA 02215, USA, Tel: 617-353-5036; Fax: 617-353-7567; barbas@bu.edu.

cognitive demands. However, there is no general agreement on the specific role of dorsolateral areas and the ACC in cognitive control (Devinsky et al., 1995; Carter et al., 1999).

To perform a task at hand successfully it is necessary to pay attention to relevant information and ignore irrelevant signals. Damage to dorsolateral areas or the ACC impairs cognitive tasks, especially in the presence of distracters (Posner and DiGirolamo, 1998; Knight et al., 1999; Rushworth et al., 2004; Lee et al., 2007). Corticocortical pathways in primates are excitatory and mainly form synapses with other excitatory neurons (White, 1989; Somogyi et al., 1998). Theoretical computational studies have proposed that interactions between excitatory neurons underlie selection of relevant signals (Wang, 2001). A smaller but significant proportion of axons from excitatory neurons form synapses with inhibitory GABAergic neurons, triggering inhibition at the site of termination. Though fewer in number than excitatory neurons, inhibitory neurons are considerably more diverse in morphology and function (Markram et al., 2004). In primates, inhibitory neurons can be grouped into three non-overlapping neurochemical classes identified by their expression of the calcium-binding proteins parvalbumin (PV), calretinin (CR), and calbindin (CB), though each class contains several morphological types (DeFelipe, 1997). PV neurons innervate the proximal dendrites, soma, or axon initial segment of other neurons, eliciting strong inhibition (DeFelipe et al., 1989b; Thomson and Deuchars, 1997). CB neurons innervate mostly distal dendrites of excitatory neurons (DeFelipe et al., 1989a; Peters and Sethares, 1997). CR neurons preferentially innervate other inhibitory neurons in the upper cortical layers, and thus have a disinhibitory role (Meskenaite, 1997; DeFelipe et al., 1999; Melchitzky et al., 2005). Disinhibition by CR neurons is thought to enhance signals, while CB neurons dampen activity at the fringes of active cortical columns to suppress noise, collectively enhancing the signal-to-noise ratio of relevant activity in working memory (Wang et al., 2004).

Prefrontal pathways may interact with these inhibitory neurons to improve response selectivity in behavioral tasks, which is disrupted after blockade of GABAergic activity (Rao et al., 1999; Rao et al., 2000). For example, microstimulation of the inter-areal pathway from prefrontal area 8 improves sensitivity to target stimuli in visual cortex by increasing their gain and decreasing noise from competing signals (Moore et al., 2003; Reynolds and Chelazzi, 2004). We reasoned that since ACC and dorsolateral areas differ in their capacity for inhibitory control in cognitive tasks, they may interact differentially with inhibitory neurons. One possibility is that the functionally distinct ACC may help reduce noise by innervating CB neurons in dorsolateral area 9, while area 46 may innervate more CR neurons and disinhibit the related area 9, particularly in the upper layers where these interneurons are most prevalent (Conde et al., 1994; Gabbott et al., 1997; Gonchar and Burkhalter, 1997; Kawaguchi and Kubota, 1997; Dombrowski et al., 2001).

The synaptic underpinnings of working memory functions for selection and suppression of signals are not known. To address this issue we investigated the synaptic organization of dorsolateral area 46 and ACC (area 32) with excitatory and inhibitory neurons in dorsolateral area 9. This design allowed us to study the synaptic pathway between two related areas with respect to working memory (dorsolateral area 46 to dorsolateral area 9), and between two distinct areas (ACC to dorsolateral area 9). We provide evidence that the ACC has more prevalent and larger synapses with inhibitory neurons in area 9, in patterns suggesting increased inhibitory control in demanding cognitive tasks.

Results

To compare the organization of two pathways, one from dorsolateral area 46 and the other from ACC (area 32), we investigated their synapses within the upper layers (I–IIIa) of area 9. Figure 1 summarizes the essence of our experimental approach. Briefly, injection of distinct

neural tracers in areas 32 (Figure 1A, grey and white), and 46 (Figure 1B, grey and black) labeled axon terminals in area 9. We examined at the light and electron microscope (EM) sites in area 9 with labeled terminals among excitatory and inhibitory neurons, which were labeled for PV, CB, or CR (Figure 1B, dotted fill and inset). Labeled terminals from the two pathways were dense in the central antero-posterior extent of area 9. Axon terminals from area 32 were diffuse and widespread, with a strong bias for the upper layers (I–IIIa; Figure 1C), and from area 46 they were more restricted and columnar, including the middle layers (IIIb–Va; Figure 1D).

Postsynaptic targets of boutons from areas 32 and 46 in layers I–IIIa of area 9

As summarized in Figure 2A, we found three major types of terminals (boutons) from axons originating in area 32 (n = 345 boutons, from three cases) and area 46 (n = 325, from two cases), based on their synapses and postsynaptic targets in area 9. The first and largest group formed single synapses with spines emerging from spiny dendrites of excitatory neurons (from area 32, 69% of labeled boutons; from area 46, 80%; Figures 2A, bouton 1; 2B, 2C and 2H; Table S1). The second group of labeled boutons innervated aspiny or sparsely spiny dendritic shafts, characteristic of cortical inhibitory neurons (area 32, 18%; area 46, 13%; Figures 2A, bouton 2; 2D, 2E and 2I). The third group consisted of multisynaptic boutons that formed synapses with two or more spines (area 32, 6%; area 46, 5%; Figures 2A, bouton 3e; 2F and 2J), or 1–2 spines and an aspiny or sparsely spiny dendritic shaft (area 32, 7%; area 46, 3%; Figures 2A, bouton 3m; 2G and 2K). Only a few labeled boutons formed synapses on shafts of spiny dendrites (≤1%). Labeled boutons that appeared to be non-synaptic varicosities were not included in this analysis (4% for area 32; 8% for area 46).

Pathway-specific distinction of presynaptic size

We classified boutons with major diameters less than 1.0 μm (2D analysis), or volumes <0.2 μm^3 (3D analysis) as small, and boutons above this size as large, based on cluster analysis ($p < 0.01$; Figures 3A–3C). Bouton size is correlated with the number of synaptic vesicles (Germuska et al., 2006) and synaptic efficacy (Murthy et al., 1997). Small boutons made up the majority in each pathway (Figure 3D, grey bars). A smaller but significant proportion of boutons were large in both pathways (Figure 3D, black bars), but in this respect the two pathways diverged. Boutons from area 32 were larger than boutons from area 46, both at the light microscope (n = 10,920 boutons from 5 cases, measured for major diameter; Figure 3A), and at the synaptic level (n = 197, 2D major diameter, Figure 3B; n = 198, 3D volume, Figure 3C; ANOVA, Bonferroni's post-hoc, $p < 0.01$). This pathway-specific difference in size was due to a larger overall size of boutons (Figures 3A–3C), as well as a higher frequency of large boutons from area 32 than from area 46 (Figures 3D–3F).

Large boutons from ACC (area 32) innervate inhibitory neurons and multiple postsynaptic sites

Further analysis revealed that the differences in bouton size depended largely on the type of postsynaptic target. In the pathway from area 32 to 9, boutons that innervated dendritic shafts of inhibitory neurons were significantly larger (>2X) than those from area 46 to 9 (two-way ANOVA, Bonferroni's post-hoc, $p < 0.01$; Figures 4A, red dots; 4B, 4H and 4I). Similarly, multisynaptic boutons from area 32 were larger (>2X) than multisynaptic boutons from area 46 ($p < 0.01$; Figures 4A, triangles; 4B, 4F, 4G, 4J and 4K). In contrast, boutons innervating single spines were comparatively uniform in size across pathways ($p = 0.84$; Figures 4A, green dots; 4B, 4D and 4E), consistent for data obtained from 3D as well as 2D EM analysis (Table S1).

Boutons from area 32 that innervated shafts of inhibitory neurons or ensembles of spines and shafts in area 9 were also more prevalent than those from area 46 ($p < 0.05$, Figure 4C; Table

S1). Overall, the pathway from area 32 to 9 formed more synapses with inhibitory neurons ($p < 0.01$, Figure 5A), through larger boutons than the pathway from area 46 to 9.

Pathway-specific innervation of distinct neurochemical classes of inhibitory neurons

The two pathways also differed in their synapses in area 9 with specific neurochemical classes of inhibitory neurons labeled for CB, PV, or CR. Boutons from area 32 formed synapses preferentially with aspiny CB+ dendrites (~49% of labeled inhibitory targets; Figures 5B and 5C), significantly more than in the pathway from area 46 to 9 (~22% of labeled targets; $p < 0.01$; Figures 5D1–D3). Axons from area 32 formed synapses with a lower but significant proportion of CR+ dendrites (~36% of labeled targets; Figures 5B, 5E and 5F). The opposite relationship was seen for the pathway from area 46 to area 9, where about half (~46%) of the labeled inhibitory targets were CR+ (Figures 5B and 5G), and CB constituted a smaller proportion. However, because axons from area 32 innervated inhibitory neurons at a higher frequency (Figure 5A), the extent of synapses with CR+ elements was comparable in the two pathways (~6% of all targets; Figure 5B). Boutons from area 32 formed fewer synapses with PV+ neurons in area 9 (~15% of labeled targets; Figures 5B and 5H) than either CB+ or CR+ neurons. In the pathway from area 46 to 9, the proportion of synapses with PV+ neurons was comparable to synapses with CB+ neurons (~28% of labeled targets; Figures 5B and 5I). The innervation of PV neurons by the two pathways is comparable to prefrontal-temporal pathways in primates (Medalla et al., 2007), but lower than in pathways linking visual areas in rats (Gonchar and Burkhalter, 2003). These findings may reflect differences in the proportion of PV inhibitory neurons, which is higher in rat visual and frontal cortices than in monkey prefrontal cortex (Conde et al., 1994; Gabbott et al., 1997; Gonchar and Burkhalter, 1997; Kawaguchi and Kubota, 1997; Dombrowski et al., 2001). The above findings indicate that the two pathways mainly differed by the higher prevalence of synapses with CB+ inhibitory neurons from the ACC than the area 46 pathway.

A majority (74–80%) of the inhibitory targets of prefrontal pathways were positive for CB, PV, or CR. A smaller proportion of inhibitory targets were morphologically identified as aspiny or sparsely spiny shafts that were immuno-negative for CB, PV, or CR, which may be attributed to weak or absent labeling of distal dendrites in the upper cortical layers, suggesting an underestimate of synapses on labeled postsynaptic sites. Alternatively, unlabeled postsynaptic sites may represent the complementary population of inhibitory neurons. For example, in triple-labeled tissue for prefrontal terminals, CB, and CR, unlabeled inhibitory targets could have been PV+. The use of serial sections helped identify and classify postsynaptic elements with a high degree of confidence. Counterbalancing staining methods using gold or TMB yielded consistent results across labeling conditions, suggesting that the pathway specificity found was not due to methodological issues.

We also used another approach to classify dendrites as spiny (excitatory) or sparsely spiny (inhibitory), especially since CB and CR also label a minority of pyramidal neurons (DeFelipe et al., 1989a; del Rio and DeFelipe, 1997). In our sample, sparsely spiny dendrites had lower spine densities (<0.5 spines/μm length) than spiny dendrites (>0.5 and up to 4 spines/μm; $p < 0.01$), consistent with previous studies (Feldman and Peters, 1978; Larkman, 1991; Kawaguchi et al., 2006). Further, the average synapse density on shafts of aspiny dendrites (2 synapses/μm), or sparsely spiny dendrites (0.6 synapses/μm) was considerably higher than for spiny dendrites, which virtually had no asymmetric shaft synapses.

Linear relationship between presynaptic and postsynaptic size

There was a linear relationship between bouton volume and postsynaptic density (PSD) area across pathways and postsynaptic targets (spine-targeting: $R^2 = 0.51$, Figure 6A; shaft-targeting: $R^2 = 0.72$, Figure 6D; volume of multisynaptic boutons versus total PSD: $R^2 = 0.7$,

not shown; $p < 0.01$; Table S1). Accordingly, boutons of comparable size that innervated spines had comparable PSD area and spine volume (bouton volume versus spine volume: $R^2 = 0.49$, Figure 6B; spine volume versus PSD: $R^2 = 0.58$, Figure 6C; $p < 0.01$; Table S1). The same relationships were found for multisynaptic boutons and their postsynaptic targets (spine volume versus PSD: $R^2 = 0.74–0.81$, $p < 0.01$). However, for boutons innervating dendritic shafts, bouton size was related to synapse size, but not dendritic size (bouton volume versus dendrite diameter: $R^2 = 0.02$, $p = 0.53$, Figure 6E; dendrite diameter versus PSD: $R^2 = 0.07$, $p = 0.21$, Figure 6F).

Comparison of labeled pathways with the surrounding neuropil

To determine whether the two pathways from areas 32 and 46 terminated in similar or distinct compartments of area 9, we used unbiased estimates of populations of unlabeled boutons forming asymmetric synapses in the neuropil around labeled boutons (White, 1989). In addition to the types of synapses seen for labeled pathways, unlabeled boutons also innervated somata (<1%), or multiple dendrites (<1%). We found a comparable proportion of unlabeled synapses with spines and dendrites as for labeled synapses in each pathway ($p > 0.05$; Table S1). However, as shown above, the two pathways differed from each other, suggesting that boutons from areas 32 and 46 terminate in distinct compartments of area 9.

Unlabeled boutons in the surrounding neuropil (mean volume ± SEM, $0.13 \pm 0.02\ \mu m^3$) were comparable in size to labeled boutons from area 46 ($p = 0.42$), but were significantly smaller ($0.12 \pm 0.01\ \mu m^3$) than boutons from area 32 ($p < 0.01$), especially those innervating dendritic shafts or multiple postsynaptic sites (Table S1). There was a higher prevalence of large multisynaptic boutons labeled from area 32 than in the surrounding neuropil (~6% of unlabeled boutons; $p < 0.01$; Table S1). Further, within the same dendritic segment, synapses from area 32 (PSD area, $0.14 \pm 0.02\ \mu m^2$) were larger than unlabeled synapses ($0.07 \pm 0.005\ \mu m^2$; $p < 0.05$), while synapses from area 46 ($0.1 \pm 0.02\ \mu m^2$) were comparable in size to unlabeled synapses ($0.1 \pm 0.03\ \mu m^2$; $p = 0.63$) on the same dendrite.

Discussion

We provide evidence that two pathways from ACC and dorsolateral area 46 differ specifically in their synapses with inhibitory neurons in dorsolateral area 9. The pathway from the functionally distinct ACC formed more and larger synapses with inhibitory neurons, and targeted preferentially the neurochemical class of calbindin inhibitory neurons, than the pathway linking the functionally related areas 46 and 9. This evidence suggests that ACC has strong influence on an inhibitory control system of dorsolateral prefrontal cortex.

Similarity of prefrontal pathways for excitation and diversity for inhibition

Both pathways innervated mostly spines of excitatory neurons in area 9, as in other corticocortical pathways (White, 1989; Callaway, 1998), and these terminals did not differ in size. The significance of the large terminals from ACC that targeted inhibitory neurons is based on evidence that bouton size is correlated with the number of synaptic vesicles (Germuska et al., 2006; Zikopoulos and Barbas, 2007) and with multivesicular release upon stimulation (Tong and Jahr, 1994; Murthy et al., 1997). This evidence suggests that ACC can effectively recruit inhibitory neurons in dorsolateral prefrontal cortex. Moreover, the ACC preferentially innervated CB inhibitory neurons, which target the distal dendrites of pyramidal neurons (DeFelipe et al., 1989a; Peters and Sethares, 1997), and are thought to decrease activity at the fringes of active cortical columns (Wang et al., 2004; Zaitsev et al., 2005). In contrast, the inhibitory targets of area 46 in area 9 were predominantly CR neurons, which innervate other GABAergic neurons in the upper layers, and thus disinhibit excitatory neurons (Meskenaite, 1997; Melchitzky et al., 2005). This evidence suggests that activation of the pathway from area

46 predominantly disinhibits activity in the related area 9, while the functionally distinct ACC enhances inhibition.

ACC stands out for its large terminals and prevalence of synapses with inhibitory neurons by comparison with other corticocortical pathways as well (Anderson et al., 1998; Anderson and Martin, 2006; Medalla et al., 2007), suggesting a distinct role in cognitive control. In contrast, synapses from area 46 with inhibitory neurons in area 9 were comparable to other corticocortical pathways, including those from area 9 to 46 (Melchitzky et al., 2001). The similarity in synapses that interlink dorsolateral areas 9 and 46 is consistent with their related function in working memory. Neurons in areas 9 and 46 are activated during selection, integration, and maintenance of relevant cues and responses in working memory tasks (Fuster, 1973; Niki and Watanabe, 1976; Tanila et al., 1992; Tanji and Hoshi, 2008). Lesions restricted to area 9 produce similar, though milder, impairments in working memory tasks than lesions of area 46 (Levy and Goldman-Rakic, 1999; Petrides, 2000), though sulcal area 46 may have a more critical role than area 9 in visuomotor tasks (Mishkin and Manning, 1978; Ono et al., 1984; Funahashi et al., 1989).

Previous studies have shown that terminals of ‘feedforward’ pathways are larger than ‘feedback’ terminals in the upper layers of the visual cortex in rats (Gonchar and Burkhalter, 1999). Here we found that axon terminals from ACC, which issues mostly feedback projections to lateral prefrontal cortex, were larger than axon terminals in the feedforward/lateral pathway from area 46 to 9 (Barbas and Rempel-Clower, 1997). The findings in the rat cortex and here suggest that there is specificity in the synaptic features of pathways, but not according to a categorical hierarchical grouping [see also (Anderson et al., 1998; Anderson and Martin, 2002; Medalla et al., 2007)]. Instead, previous studies have shown a graded increase in the size of boutons from layer I through the middle (lower III-upper V) cortical layers (Germuska et al., 2006; Medalla et al., 2007).

The ACC and dorsolateral prefrontal cortex in cognitive control

Figure 7 summarizes how the synaptic diversity of pathways from ACC (area 32) and dorsolateral area 46 may differentially affect neuronal dynamics in area 9. Prefrontal pathways predominantly engage excitatory neurons (Figure 7, green), which carry either task-relevant signals, or noise (Wang, 1999;Gonzalez-Burgos et al., 2000;Constantinidis et al., 2001;Abbott and Chance, 2005). Our findings suggest that the functionally distinct prefrontal pathways are similar in enhancing signal but differ in their ability to suppress noise. Specifically, the two pathways innervated to a similar extent CR inhibitory neurons, which disinhibit excitatory neurons, and may thus enhance task-relevant signals in working memory (Wang et al., 2004). On the other hand, ACC had a bigger influence on CB inhibitory neurons, which are thought to suppress irrelevant signals and consequently increase the signal-to-noise ratio of task-relevant activity. In simple working memory tasks, the few CB neurons engaged by area 46 may suffice to suppress moderate noise (Figure 7A, 46-cb). However, the ACC is recruited when noise increases under high cognitive demands (MacDonald, III et al., 2000;Gehring and Knight, 2000;Ito et al., 2003;Badre and Wagner, 2004;Johnston et al., 2007;Chen et al., 2008;Emeric et al., 2008). The ACC pathway may help reduce excessive noise by strongly activating CB inhibitory neurons through large terminals (Figure 7B, 32-cb).

The ACC is also involved in monitoring error, switching attention, or reversing decisions (Ito et al., 2003; Johnston et al., 2007; Schall et al., 2002; Bechtereva et al., 2005). The efficient large terminals from area 32 may provide the synaptic substrate for these functions as well (Figure 7C). Through its synapses with CB neurons, the ACC may override activity of a previous, but now undesired, signal, and through its synapses with CR neurons may disinhibit a new signal, essentially overcoming the weaker synaptic impact of the smaller terminals from area 46 (Figure 7C, 32-cb overpowers 46-cr, 32-cr overpowers 46-cb).

Fast-spiking PV inhibitory neurons influence the timing of signals for working memory tasks (Rao et al., 1999; Constantinidis et al., 2002) and may also be involved in these functions, though they were not the major inhibitory targets in the two pathways. This finding is consistent with the lower prevalence of PV inhibitory neurons in the upper layers (DeFelipe, 1997), suggesting that they may have a greater influence in the middle-deep cortical layers, where they are most abundant. Nevertheless, the large terminals from ACC onto PV neurons (Figure 7C, 32-pv) may provide excitatory drive (Gonzalez-Burgos et al., 2004; Abbott and Chance, 2005) to shift the temporal dynamics and reverse a response. This process may also be facilitated by the unusual class of large multisynaptic boutons, which were specific to the ACC pathway, and formed synapses with inhibitory and excitatory neurons (Figure 4J). The above circuit model is oversimplified, and understanding the conditions for recruitment of these pathways in behavior ultimately rests in the realm of physiology in awake primates.

The ACC is linked with the hippocampus, amygdala, hypothalamus, orbitofrontal and medial temporal cortices, which are associated with long-term memory and emotions (Barbas et al., 2002). In contrast, dorsolateral prefrontal areas have sparse connections with limbic structures and likely access mnemonic and affective information through their extensive connections with ACC (Barbas, 2000). At the functional level, motivation and reward improve working memory by strengthening task-related activity in lateral prefrontal areas (Watanabe, 2007). In contrast, stress-related stimuli impair working memory (Arnsten, 2007), and unrewarded actions are subsequently avoided (Taylor et al., 2006).

Our findings address the much debated issue of the relative contribution of ACC and dorsolateral prefrontal cortex in cognitive control at the synaptic level. Specifically, the synaptic interactions suggest that the ACC may use affective and mnemonic information to either act synergistically with dorsolateral prefrontal areas and strengthen a relevant signal when noise intrudes, or reverse undesired decisions for flexible behavior (Bush et al., 2000; Paus, 2001; Matsumoto and Tanaka, 2004; Watanabe, 2007) in functions that are severely affected in schizophrenia (Vogels and Abbott, 2007; Allen et al., 2008). The density of inhibitory neurons is reduced in the upper layers of ACC in the brains of schizophrenic patients (Reynolds et al., 2001; Benes and Berretta, 2001). In contrast, in the deep layers PV inhibitory neurons are either increased in density or unchanged (Kalus et al., 1997; Cotter et al., 2002), but pyramidal (excitatory) neurons decrease (Benes et al., 2001). Functional imaging studies show hypofunction of ACC in schizophrenic patients (Fletcher et al., 1999; Kerns et al., 2005; Allen et al., 2007), consistent with the anatomic data, as well as evidence on the combined contribution of excitatory and inhibitory neurons to the BOLD signal (Logothetis and Wandell, 2004; Buzsaki et al., 2007).

Our findings place the emphasis on a deficiency in pathways, rather than cortical locus, in schizophrenia. Specifically, the deep layers of ACC, which show reduction in excitatory neurons in schizophrenia, are also the major source of projections to the upper layers of dorsolateral prefrontal areas in non-human primates (Barbas and Rempel-Clower, 1997). The present data provide a circuit mechanism to suggest that pathology in the deep layers of ACC reduces excitatory drive on inhibitory neurons of dorsolateral prefrontal cortices, perturbing the delicate balance of excitation and inhibition.

Experimental Procedures

Subjects

Animals were obtained from the New England Primate Research Center (NEPRC) and protocols were approved by the Institutional Animal Care and Use Committee at NEPRC, Harvard Medical School, and Boston University School of Medicine in accordance with NIH

guidelines (DHEW Publication no. [NIH] 80-22, revised 1987, Office of Science and Health Reports, DRR/NIH, Bethesda, MD, USA).

Surgical procedures and injection of neural tracers

Tracer injections were made in normal rhesus monkeys (*Macaca mulatta*; 2–3 years of age, n = 5) under general anesthesia. A small region of the prefrontal cortex was exposed to inject areas 32 and 46 (Figure 1) with the neural tracers, biotinylated dextran amine (BDA), fluoroemerald (FE, dextran fluorescein), or fluororuby (FR, dextran tetramethylrhodamine; Molecular Probes, Eugene, OR), all 10000 MW to optimize anterograde over retrograde transport (Reiner et al., 2000). In each case, the dye was diluted to 10 mg/ml and delivered in 2–4 penetrations at a depth of 1.2–1.6 mm below the pial surface.

After a survival period of 18 days, the animals were anesthetized with a lethal dose of sodium pentobarbital (>50 mg/kg, to effect) and transcardially perfused with 4% paraformaldehyde and 0.2% glutaraldehyde in 0.1 M PB (pH 7.4). The brain was removed, cryoprotected, frozen in −75°C isopentane, and cut in the coronal plane at 50 μm, as described (Medalla et al., 2007). Tissue was stored in anti-freeze solution (30% ethylene glycol, 30% glycerol, 40% 0.05 M PB, pH 7.4 with 0.05% sodium azide) at −20°C until use.

Immunohistochemistry for light microscopy

Assays were conducted on free-floating sections (at 4°C). Sections were incubated in 0.05 M glycine and preblocked in 5% normal goat serum (NGS) and 5% bovine serum albumin (BSA) with 0.2% Triton-X. To view BDA label, sections were incubated in an avidin biotin (AB) horseradish peroxidase (HRP) complex (1 hr, 1:100 in PBS with 0.1% Triton X; PK-6100 ABC kit, Vector Labs, Burlingame, CA), and processed with diaminobenzidine (DAB, 2–3 min; Zymed Labs, South San Francisco, CA). To view fluorescent tracers (FE and FR) under brightfield illumination, we incubated sections in AB blocking reagent (Vector) to prevent cross-reaction with BDA injected in the same animal, and used antibodies against FE or FR (1:800, in PBS, 1% NGS, 1% BSA, 0.1% Triton-X; rabbit polyclonal, Molecular Probes; overnight incubation). Sections were incubated in biotinylated goat anti-rabbit IgG (2 hr, 1:200; Vector), then in AB-HRP, and DAB. In some sections, FE or FR labeling was visualized using the peroxidase-anti-peroxidase (PAP) method, which does not involve biotinylated secondary antibodies (Zikopoulos and Barbas, 2006), and yielded similar label.

Preembedding immunohistochemistry for EM

For viewing synapses of labeled prefrontal pathways with CB, PV, or CR postsynaptic sites at the EM, we employed preembedding immunohistochemistry using gold-conjugated antibodies. Sections were processed for BDA, FE, or FR using DAB, with 0.025% Triton-X. Sections were incubated overnight in primary antibody for CB (1:2000; mouse monoclonal, Swant, Bellinzona, Switzerland), PV (1:2000; mouse monoclonal, Chemicon, Temecula, CA; rabbit polyclonal, Swant), or CR (1:2000; mouse monoclonal; rabbit polyclonal, Swant), then overnight in gold-conjugated secondary goat anti-mouse or anti-rabbit IgG (1:50, 1 nm gold particle diameter; Amersham Biosciences, Piscataway, NJ). Sections were postfixed with 2% or 6% glutaraldehyde as described (Medalla et al., 2007). Gold labeling was then intensified using a silver enhancement kit (6–12 min; IntenSE M kit, Amersham), which results in aggregates of gold particles of variable sizes.

For triple labeling, we combined DAB (uniform label), gold staining with silver enhancement (clumps of gold particles), and tetramethylbenzidine (TMB) staining (rod-shaped precipitate), which are easily differentiated in EM. After labeling fibers with DAB, sections were incubated in AB blocking reagent to prevent cross-reaction with TMB. For BDA labeled tissue, sections were co-incubated overnight in the primary antibodies for PV or CR (rabbit polyclonal) and

CB (mouse monoclonal), and then in biotinylated anti-mouse IgG, followed by AB-HRP. For FE or FR labeled tissue, we used a combination of two mouse monoclonal primary antibodies for PV, CB, or CR, processed successively, using the Mouse-on-Mouse blocking kit (M.O.M. basic kit, Vector) in between to prevent cross-reaction. Sections were incubated overnight in the appropriate gold-conjugated IgG, postfixed, and intensified with silver. Sections were processed for TMB, then stabilized with DAB-cobalt chloride solution, as described (Medalla et al., 2007). In control experiments, we omitted primary antibodies to test the specificity of secondary antibodies, and used the AB blocking kit prior to AB binding, and the M.O.M. kit prior to secondary antibody binding.

Small pieces of cortex with label in area 9 were then cut from sites with no retrograde label in the vicinity, to avoid the possibility of sampling local axon collaterals of labeled neurons. The tissue pieces were postfixed in osmium, dehydratedin ethanol (50–100%), stained with 1% uranyl acetate, infiltrated with propylene oxide, and flat-embedded in araldite resin, as described (Medalla et al., 2007).

Data analysis

Bouton size measurement: light microscope—To measure boutons at the light microscope, we captured images at high magnification (1000×) of 1–2 random sites within a region of anterograde labeling in layers I and II-IIIa of area 9, with a CCD camera (Olympus DP70) mounted on a microscope (Olympus BX51), as described (Zikopoulos and Barbas, 2006). We measured the maximum major diameters of each labeled profile within each image using ImageJ (v. 1.32j for Windows, NIH, USA). Our sampling included measurement of ~5,000 boutons from 2–3 cases for each pathway.

Mapping labeled synapses—To map synapses formed by prefrontal axons, re-embedded blocks of tissue from layers I (n = 13 pieces) and II-IIIa (n = 9 pieces) were trimmed with a diamond trim tool (Diatome, Fort Washington, PA; layer I, average block face area = 161 × 285 μm; II-IIIa, 261 × 456 μm) for serial sectioning at 50 nm, as described (Medalla et al., 2007). We examined sections at 60 kV with a transmission EM (100CX;Jeol, Peabody, MA), photographed at 10,000× or 6,500×, and scanned the negatives (Epson Perfection 4990 Photo Scanner, Epson America, Inc., Long Beach, CA).

We conducted systematic and exhaustive sampling of labeled boutons from an average of 100 serial sections from each piece of tissue to yield a comparable sample of labeled boutons per pathway and neurochemical stain. Overall we identified about 300 labeled boutons from each pathway (n = 670 total from 5 cases), with 198 boutons used for 3D analysis to measure volumes (>90% of which were synaptic), 197 for 2D analysis of major diameter, and the rest were used only to identify postsynaptic targets.

3D reconstruction of synapses—We used the open source program Reconstruct [www.bu.edu/neural; (Fiala, 2005)] to analyze labeled boutons and their postsynaptic targets and reconstruct them in 3D from serial sections (30–50 sections for each synapse). The thickness of sections was estimated using the method of cylindrical diameters (Fiala and Harris, 2001a). Object contours of boutons and postsynaptic elements were manually traced section-by-section, and used to calculate volume and surface area. A 3D model was generated and imported in 3D Studio Max (v3, Autodesk Inc., San Rafael, CA) for additional rendering.

We used classic criteria to identify synapses on spines, which are enriched on excitatory neurons, or with aspiny or sparsely spiny shafts, which are characteristic of inhibitory neurons in the cortex (Peters et al., 1991). We identified postsynaptic targets labeled with CB, CR, or PV by the presence of gold or TMB within the postsynaptic target in about a fourth of the sections in the series (Figure S1). CB and CR are expressed in a minority of pyramidal neurons

(DeFelipe et al., 1989a; del Rio and DeFelipe, 1997). We considered postsynaptic targets as belonging to CB or CR inhibitory neurons if they were labeled, and also were aspiny or sparsely spiny. The latter were characterized by computing a spine and synapse density index of reconstructed dendrites, as described (Fiala and Harris, 2001b).

We used stereologic methods to compare labeled boutons with unlabeled boutons forming asymmetric synapses in the surrounding neuropil. We employed systematic random sampling of the neuropil surrounding 1 in every 30 labeled boutons from each block of tissue from 4 cases. In each termination site of 30–50 serial sections (average volume = 272 μm^3; n = 5 sites surrounding area 32 boutons; n = 6 sites around area 46), labeled boutons were photographed at the center of the frame and unlabeled boutons around it were exhaustively counted (n = 1,604). Unlabeled boutons that were complete in the series were reconstructed in 3D (n = 172). The average total volume of tissue analyzed was about 1.5 mm^3 for each pathway.

2D measurements of synapses—Labeled boutons and their postsynaptic targets were identified, photographed, and sampled exhaustively in every 10 adjacent sections at intervals of 1 μm (skipping 20 sections) throughout the entire series. This sampling is comparable to 2D single-section EM analysis described previously (Germuska et al., 2006), but ambiguity is reduced by having essentially nine ‘look-up’ sections, instead of the standard 2–3 sections. We used ImageJ to measure the maximum major diameters of labeled boutons at the level of the synapse within the 10-section sampling interval.

Statistical analysis—For each injection site, measurements were made from multiple sites in layers I-IIIa of area 9 in 2–3 monkeys, as described above. Comparisons were made using one-way or two-way ANOVA and Bonferroni’s post-hoc in Statistica (v.7 for Windows, StatSoft Inc., Tulsa, OK) or SPSS (v.10.1 for Windows, SPSS Inc., Chicago, IL). Linear regression was conducted using Least–Squares Approximation in Sigma-Plot (v.7.0, SPSS Inc.). Linear relationships were consistent between layers and pathways, so the data were pooled. To determine the proportion of large and small boutons, we performed K-means cluster analysis on the major diameters and volumes of labeled boutons using Statistica, with parameters set to maximize initial between-cluster differences. For cluster analyses, no differences were found between layers or between light microscopy and EM, so the data were combined.

Supplementary Material

Refer to Web version on PubMed Central for supplementary material.

Acknowledgments

We thank Dr. Ron Killiany for imaging; Marcia Feinberg, Kim Ang, and Sue Paul for technical assistance; Dr. John Fiala for help with 3D reconstruction; Dr. Alan Peters for advice with EM; and Dr. Basilis Zikopoulos, Dr. Jamie G. Bunce, and Michelle Hogle for comments on the manuscript. Supported by NIH grants from NINDS and NIMH.

References

Abbott LF, Chance FS. Drivers and modulators from push-pull and balanced synaptic input. Prog Brain Res 2005;149:147–155. [PubMed: 16226582]

Allen P, Amaro E, Fu CH, Williams SC, Brammer MJ, Johns LC, McGuire PK. Neural correlates of the misattribution of speech in schizophrenia. Br J Psychiatry 2007;190:162–169. [PubMed: 17267934]

Allen P, Laroi F, McGuire PK, Aleman A. The hallucinating brain: A review of structural and functional neuroimaging studies of hallucinations. Neurosci Biobehav Rev 2008;32:175–191. [PubMed: 17884165]

Anderson JC, Binzegger T, Martin KA, Rockland KS. The connection from cortical area V1 to V5: a light and electron microscopic study. J Neurosci 1998;18:10525–10540. [PubMed: 9852590]

Anderson JC, Martin KA. Connection from cortical area V2 to MT in macaque monkey. J Comp Neurol 2002;443:56–70. [PubMed: 11793347]

Anderson JC, Martin KA. Synaptic connection from cortical area V4 to V2 in macaque monkey. J Comp Neurol 2006;495:709–721. [PubMed: 16506191]

Arnsten AF. Catecholamine and second messenger influences on prefrontal cortical networks of "representational knowledge": a rational bridge between genetics and the symptoms of mental illness. Cereb Cortex 2007;17(Suppl 1):i6–15. [PubMed: 17434919]

Badre D, Wagner AD. Selection, integration, and conflict monitoring; assessing the nature and generality of prefrontal cognitive control mechanisms. Neuron 2004;41:473–487. [PubMed: 14766185]

Barbas H. Complementary role of prefrontal cortical regions in cognition, memory and emotion in primates. Adv Neurol 2000;84:87–110. [PubMed: 11091860]

Barbas, H.; Ghashghaei, H.; Rempel-Clower, N.; Xiao, D. Anatomic basis of functional specialization in prefrontal cortices in primates. In: Grafman, J., editor. Handbook of Neuropsychology. Amsterdam: Elsevier Science B.V; 2002. p. 1-27.

Barbas H, Rempel-Clower N. Cortical structure predicts the pattern of corticocortical connections. Cereb Cortex 1997;7:635–646. [PubMed: 9373019]

Bechtereva NP, Shemyakina NV, Starchenko MG, Danko SG, Medvedev SV. Error detection mechanisms of the brain: background and prospects. Int J Psychophysiol 2005;58:227–234. [PubMed: 16169106]

Benes FM, Berretta S. GABAergic interneurons: implications for understanding schizophrenia and bipolar disorder. Neuropsychopharmacology 2001;25:1–27. [PubMed: 11377916]

Benes FM, Vincent SL, Todtenkopf M. The density of pyramidal and nonpyramidal neurons in anterior cingulate cortex of schizophrenic and bipolar subjects. Biol Psychiatry 2001;50:395–406. [PubMed: 11566156]

Bush G, Luu P, Posner MI. Cognitive and emotional influences in anterior cingulate cortex. Trends Cogn Sci 2000;4:215–222. [PubMed: 10827444]

Buzsaki G, Kaila K, Raichle M. Inhibition and brain work. Neuron 2007;56:771–783. [PubMed: 18054855]

Callaway EM. Local circuits in primary visual cortex of the macaque monkey. Annu Rev Neurosci 1998;21:47–74. [PubMed: 9530491]

Carter CS, Botvinick MM, Cohen JD. The contribution of the anterior cingulate cortex to executive processes in cognition. Rev Neurosci 1999;10:49–57. [PubMed: 10356991]

Chen A, Xu P, Wang Q, Luo Y, Yuan J, Yao D, Li H. The timing of cognitive control in partially incongruent categorization. Hum Brain Mapp 2008;29:1028–1039. [PubMed: 17894393]

Condé F, Lund JS, Jacobowitz DM, Baimbridge KG, Lewis DA. Local circuit neurons immunoreactive for calretinin, calbindin D-28k or parvalbumin in monkey prefrontal cortex: distribution and morphology. J Comp Neurol 1994;341:95–116. [PubMed: 8006226]

Constantinidis C, Franowicz MN, Goldman-Rakic PS. Coding specificity in cortical microcircuits: a multiple-electrode analysis of primate prefrontal cortex. J Neurosci 2001;21:3646–3655. [PubMed: 11331394]

Constantinidis C, Williams GV, Goldman-Rakic PS. A role for inhibition in shaping the temporal flow of information in prefrontal cortex. Nat Neurosci 2002;5:175–180. [PubMed: 11802172]

Cotter D, Landau S, Beasley C, Stevenson R, Chana G, MacMillan L, Everall I. The density and spatial distribution of GABAergic neurons, labelled using calcium binding proteins, in the anterior cingulate cortex in major depressive disorder, bipolar disorder, and schizophrenia. Biol Psychiatry 2002;51:377–386. [PubMed: 11904132]

DeFelipe J. Types of neurons, synaptic connections and chemical characteristics of cells immunoreactive for calbindin-D28K, parvalbumin and calretinin in the neocortex. J Chem Neuroanat 1997;14:1–19. [PubMed: 9498163]

DeFelipe J, Gonzalez-Albo MC, del Rio MR, Elston GN. Distribution and patterns of connectivity of interneurons containing calbindin, calretinin, and parvalbumin in visual areas of the occipital and temporal lobes of the macaque monkey. J Comp Neurol 1999;412:515–526. [PubMed: 10441237]

DeFelipe J, Hendry SH, Jones EG. Synapses of double bouquet cells in monkey cerebral cortex visualized by calbindin immunoreactivity. Brain Res 1989a;503:49–54. [PubMed: 2611658]

DeFelipe J, Hendry SH, Jones EG. Visualization of chandelier cell axons by parvalbumin immunoreactivity in monkey cerebral cortex. Proc Natl Acad Sci U S A 1989b;86:2093–2097. [PubMed: 2648389]

del Rio MR, DeFelipe J. Synaptic connections of calretinin-immunoreactive neurons in the human neocortex. J Neurosci 1997;17(13):5143–5154. [PubMed: 9185552]

Devinsky O, Morrell MJ, Vogt BA. Contributions of anterior cingulate cortex to behaviour. Brain 1995;118:279–306. [PubMed: 7895011]

Dombrowski SM, Hilgetag CC, Barbas H. Quantitative architecture distinguishes prefrontal cortical systems in the rhesus monkey. Cereb Cortex 2001;11:975–988. [PubMed: 11549620]

Emeric EE, Brown JW, Leslie M, Pouget P, Stuphorn V, Schall JD. Performance monitoring local field potentials in the medial frontal cortex of primates: anterior cingulate cortex. J Neurophysiol 2008;99:759–772. [PubMed: 18077665]

Feldman ML, Peters A. The forms of non-pyramidal neurons in the visual cortex of the rat. J Comp Neurol 1978;179:761–793. [PubMed: 346619]

Fiala JC. Reconstruct: a free editor for serial section microscopy. J Microsc 2005;218:52–61. [PubMed: 15817063]

Fiala JC, Harris KM. Cylindrical diameters method for calibrating section thickness in serial electron microscopy. J Microsc 2001a;202:468–472. [PubMed: 11422668]

Fiala JC, Harris KM. Extending unbiased stereology of brain ultrastructure to three- dimensional volumes. J Am Med Inform Assoc 2001b;8:1–16. [PubMed: 11141509]

Fletcher P, McKenna PJ, Friston KJ, Frith CD, Dolan RJ. Abnormal cingulate modulation of fronto-temporal connectivity in schizophrenia. Neuroimage 1999;9:337–342. [PubMed: 10075903]

Funahashi S, Bruce CJ, Goldman-Rakic PS. Mnemonic coding of visual space in the monkey's dorsolateral prefrontal cortex. J Neurophysiol 1989;61:331–349. [PubMed: 2918358]

Fuster JM. Unit activity in prefrontal cortex during delayed-response performance: neuronal correlates of transient memory. J Neurophysiol 1973;36:61–78. [PubMed: 4196203]

Gabbott PL, Dickie BG, Vaid RR, Headlam AJ, Bacon SJ. Local-circuit neurons in the medial prefrontal cortex (areas 25, 32 and 24b) in the rat: morphology and quantitative distribution. J Comp Neurol 1997;377:465–499. [PubMed: 9007187]

Gehring WJ, Knight RT. Prefrontal-cingulate interactions in action monitoring. Nat Neurosci 2000;3:516–520. [PubMed: 10769394]

Germuska M, Saha S, Fiala J, Barbas H. Synaptic distinction of laminar specific prefrontal-temporal pathways in primates. Cereb Cortex 2006;16:865–875. [PubMed: 16151179]

Goldman-Rakic PS. Cellular basis of working memory. Neuron 1995;14:477–485. [PubMed: 7695894]

Gonchar Y, Burkhalter A. Three distinct families of GABAergic neurons in rat visual cortex. Cereb Cortex 1997;7:347–358. [PubMed: 9177765]

Gonchar Y, Burkhalter A. Differential subcellular localization of forward and feedback interareal inputs to parvalbumin expressing GABAergic neurons in rat visual cortex. J Comp Neurol 1999;406:346–360. [PubMed: 10102500]

Gonchar Y, Burkhalter A. Distinct GABAergic targets of feedforward and feedback connections between lower and higher areas of rat visual cortex. J Neurosci 2003;23:10904–10912. [PubMed: 14645486]

Gonzalez-Burgos G, Barrionuevo G, Lewis DA. Horizontal synaptic connections in monkey prefrontal cortex: an in vitro electrophysiological study. Cereb Cortex 2000;10:82–92. [PubMed: 10639398]

Gonzalez-Burgos G, Krimer LS, Urban NN, Barrionuevo G, Lewis DA. Synaptic Efficacy during Repetitive Activation of Excitatory Inputs in Primate Dorsolateral Prefrontal Cortex. Cereb Cortex 2004;14:530–542. [PubMed: 15054069]

Ito S, Stuphorn V, Brown JW, Schall JD. Performance monitoring by the anterior cingulate cortex during saccade countermanding. Science 2003;302:120–122. [PubMed: 14526085]

Johnston K, Levin HM, Koval MJ, Everling S. Top-down control-signal dynamics in anterior cingulate and prefrontal cortex neurons following task switching. Neuron 2007;53:453–462. [PubMed: 17270740]

Kalus P, Senitz D, Beckmann H. Altered distribution of parvalbumin-immunoreactive local circuit neurons in the anterior cingulate cortex of schizophrenic patients. Psychiatry Res 1997;75:49–59. [PubMed: 9287373]

Kawaguchi Y, Karube F, Kubota Y. Dendritic branch typing and spine expression patterns in cortical nonpyramidal cells. Cereb Cortex 2006;16:696–711. [PubMed: 16107588]

Kawaguchi Y, Kubota Y. GABAergic cell subtypes and their synaptic connections in rat frontal cortex. Cereb Cortex 1997;7:476–486. [PubMed: 9276173]

Kerns JG, Cohen JD, MacDonald AW III, Johnson MK, Stenger VA, Aizenstein H, Carter CS. Decreased conflict- and error-related activity in the anterior cingulate cortex in subjects with schizophrenia. Am J Psychiatry 2005;162:1833–1839. [PubMed: 16199829]

Knight RT, Staines WR, Swick D, Chao LL. Prefrontal cortex regulates inhibition and excitation in distributed neural networks. Acta Psychol (Amst) 1999;101:159–178. [PubMed: 10344184]

Larkman AU. Dendritic morphology of pyramidal neurones of the visual cortex of the rat: III. Spine distributions. J Comp Neurol 1991;306:332–343. [PubMed: 1711059]

Lee D, Rushworth MF, Walton ME, Watanabe M, Sakagami M. Functional specialization of the primate frontal cortex during decision making. J Neurosci 2007;27:8170–8173. [PubMed: 17670961]

Levy R, Goldman-Rakic PS. Association of storage and processing functions in the dorsolateral prefrontal cortex of the nonhuman primate. J Neurosci 1999;19:5149–5158. [PubMed: 10366648]

Logothetis NK, Wandell BA. Interpreting the BOLD signal. Annu Rev Physiol 2004;66:735–769. [PubMed: 14977420]

MacDonald AW III, Cohen JD, Stenger VA, Carter CS. Dissociating the role of the dorsolateral prefrontal and anterior cingulate cortex in cognitive control. Science 2000;288:1835–1838. [PubMed: 10846167]

Markram H, Toledo-Rodriguez M, Wang Y, Gupta A, Silberberg G, Wu C. Interneurons of the neocortical inhibitory system. Nat Rev Neurosci 2004;5:793–807. [PubMed: 15378039]

Matsumoto K, Tanaka K. The role of the medial prefrontal cortex in achieving goals. Curr Opin Neurobiol 2004;14:178–185. [PubMed: 15082322]

Medalla M, Lera P, Feinberg M, Barbas H. Specificity in inhibitory systems associated with prefrontal pathways to temporal cortex in primates. Cereb Cortex 2007;17(Suppl 1):i136–i150. [PubMed: 17725996]

Melchitzky DS, Eggan SM, Lewis DA. Synaptic targets of calretinin-containing axon terminals in macaque monkey prefrontal cortex. Neuroscience 2005;130:185–195. [PubMed: 15561434]

Melchitzky DS, Gonzalez-Burgos G, Barrionuevo G, Lewis DA. Synaptic targets of the intrinsic axon collaterals of supragranular pyramidal neurons in monkey prefrontal cortex. J Comp Neurol 2001;430:209–221. [PubMed: 11135257]

Meskenaite V. Calretinin-immunoreactive local circuit neurons in area 17 of the cynomolgus monkey, Macaca fascicularis. J Comp Neurol 1997;379:113–132. [PubMed: 9057116]

Mishkin M, Manning FJ. Non-spatial memory after selective prefrontal lesions in monkeys. Brain Res 1978;143:313–323. [PubMed: 415803]

Moore T, Armstrong KM, Fallah M. Visuomotor origins of covert spatial attention. Neuron 2003;40:671–683. [PubMed: 14622573]

Muller NG, Knight RT. The functional neuroanatomy of working memory: contributions of human brain lesion studies. Neuroscience 2006;139:51–58. [PubMed: 16352402]

Murthy VN, Sejnowski TJ, Stevens CF. Heterogeneous release properties of visualized individual hippocampal synapses. Neuron 1997;18:599–612. [PubMed: 9136769]

Niki H, Watanabe M. Prefrontal unit activity and delayed response: relation to cue location versus direction of response. Brain Res 1976;105:79–89. [PubMed: 1252960]

Ono T, Nishino H, Fukuda M, Sasaki K, Nishijo N. Single neuron activity in dorsolateral prefrontal cortex of monkey during operant behavior sustanined by food reward. Brain Res 1984;311:323–332. [PubMed: 6498489]

Paus T. Primate anterior cingulate cortex: where motor control, drive and cognition interface. Nat Rev Neurosci 2001;2:417–424. [PubMed: 11389475]

Peters, A.; Palay, SL.; Webster, HD. Neurons and their supporting cells. New York: Oxford University Press; 1991. The fine structure of the nervous system.

Peters A, Sethares C. The organization of double bouquet cells in monkey striate cortex. J Neurocytol 1997;26:779–797. [PubMed: 9482155]

Petrides M. The role of the mid-dorsolateral prefrontal cortex in working memory. Exp Brain Res 2000;133:44–54. [PubMed: 10933209]

Posner, MI.; DiGirolamo, GJ. Executive attention: conflict, target detection, and cognitive control. In: Parasuraman, R., editor. The attentive brain. Cambridge: The MIT Press; 1998. p. 401-423.

Rao SG, Williams GV, Goldman-Rakic PS. Isodirectional tuning of adjacent interneurons and pyramidal cells during working memory: evidence for microcolumnar organization in PFC. J Neurophysiol 1999;81:1903–1916. [PubMed: 10200225]

Rao SG, Williams GV, Goldman-Rakic PS. Destruction and creation of spatial tuning by disinhibition: GABA(A) blockade of prefrontal cortical neurons engaged by working memory. J Neurosci 2000;20:485–494. [PubMed: 10627624]

Reiner A, Veenman CL, Medina L, Jiao Y, Del Mar N, Honig MG. Pathway tracing using biotinylated dextran amines. J Neurosci Methods 2000;103:23–37. [PubMed: 11074093]

Reynolds GP, Zhang ZJ, Beasley CL. Neurochemical correlates of cortical GABAergic deficits in schizophrenia: selective losses of calcium binding protein immunoreactivity. Brain Res Bull 2001;55:579–584. [PubMed: 11576754]

Reynolds JH, Chelazzi L. Attentional modulation of visual processing. Annu Rev Neurosci 2004;27:611–647. [PubMed: 15217345]

Rushworth MF, Walton ME, Kennerley SW, Bannerman DM. Action sets and decisions in the medial frontal cortex. Trends Cogn Sci 2004;8:410–417. [PubMed: 15350242]

Schall JD, Stuphorn V, Brown JW. Monitoring and control of action by the frontal lobes. Neuron 2002;36:309–322. [PubMed: 12383784]

Somogyi P, Tamas G, Lujan R, Buhl EH. Salient features of synaptic organisation in the cerebral cortex. Brain Res Brain Res Rev 1998;26:113–135. [PubMed: 9651498]

Tanila H, Carlson S, Linnankoski I, Lindroos F, Kahila H. Functional properties of dorsolateral prefrontal cortical neurons in awake monkey. Behav Brain Res 1992;47:169–180. [PubMed: 1590947]

Tanji J, Hoshi E. Role of the lateral prefrontal cortex in executive behavioral control. Physiol Rev 2008;88:37–57. [PubMed: 18195082]

Taylor SF, Martis B, Fitzgerald KD, Welsh RC, Abelson JL, Liberzon I, Himle JA, Gehring WJ. Medial frontal cortex activity and loss-related responses to errors. J Neurosci 2006;26:4063–4070. [PubMed: 16611823]

Thomson AM, Deuchars J. Synaptic interactions in neocortical local circuits: dual intracellular recordings in vitro. Cereb Cortex 1997;7:510–522. [PubMed: 9276176]

Tong G, Jahr CE. Multivesicular release from excitatory synapses of cultured hippocampal neurons. Neuron 1994;12:51–59. [PubMed: 7507341]

Vogels TP, Abbott LF. Gating deficits in model networks: a path to schizophrenia? Pharmacopsychiatry 2007;40(Suppl 1):S73–S77. [PubMed: 18080946]

Wang XJ. Synaptic basis of cortical persistent activity: the importance of NMDA receptors to working memory. J Neurosci 1999;19:9587–9603. [PubMed: 10531461]

Wang XJ. Synaptic reverberation underlying mnemonic persistent activity. Trends Neurosci 2001;24:455–463. [PubMed: 11476885]

Wang XJ, Tegner J, Constantinidis C, Goldman-Rakic PS. Division of labor among distinct subtypes of inhibitory neurons in a cortical microcircuit of working memory. Proc Natl Acad Sci U S A 2004;101:1368–1373. [PubMed: 14742867]

Watanabe M. Role of anticipated reward in cognitive behavioral control. Curr Opin Neurobiol 2007;17:213–219. [PubMed: 17336512]

White, EL. Structure, function and theory. Boston: Birkhäuser; 1989. Cortical circuits. Synaptic organization of the cerebral cortex.

Zaitsev A, Gonzalez-Burgos G, Povysheva N, Kroner S, Lewis D, Krimer L. Localization of calcium-binding proteins in physiologically and morphologically characterized interneurons of monkey dorsolateral prefrontal cortex. Cereb Cortex 2005;15:1178–1186. [PubMed: 15590911]

Zikopoulos B, Barbas H. Prefrontal projections to the thalamic reticular nucleus form a unique circuit for attentional mechanisms. J Neurosci 2006;26:7348–7361. [PubMed: 16837581]

Zikopoulos, B.; Barbas, H. PLoS One. Vol. 2. 2007. Parallel Driving and Modulatory Pathways Link the Prefrontal Cortex and Thalamus; p. e848

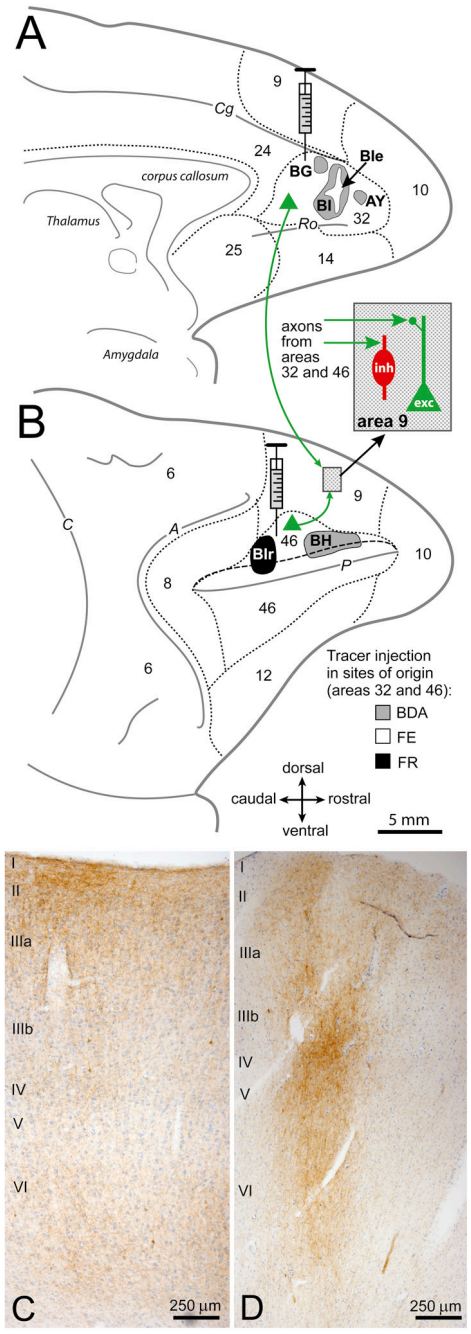

Figure 1. Tracing pathways from ACC (area 32) and area 46 to area 9

(A) Axon terminals in area 9 were labeled after injection of distinct neural tracers in ACC area 32 (cases AY, BG, BI and BIe) shown on the medial surface of the rhesus monkey brain; and **(B)** in dorsolateral area 46 (cases BIr and BH) on the lateral surface (long dashes depict the upper bank of the principal sulcus). Short dashes mark areal borders. The inset in B shows the location of sites examined in area 9 with labeled axon terminals (green arrows) among excitatory (exc, green) and inhibitory (inh, red) neurons.

(C–D) Coronal sections show labeled axon terminals (brown) in area 9: **(C)** from ACC (area 32) and; **(D)** from area 46. Sections were counterstained with Nissl (blue) to show cortical

layers; laminar labels are placed at the beginning of each cortical layer. Abbreviations of sulci: A, arcuate; C, central; Cg, cingulate; P, principal; Ro, rostral.

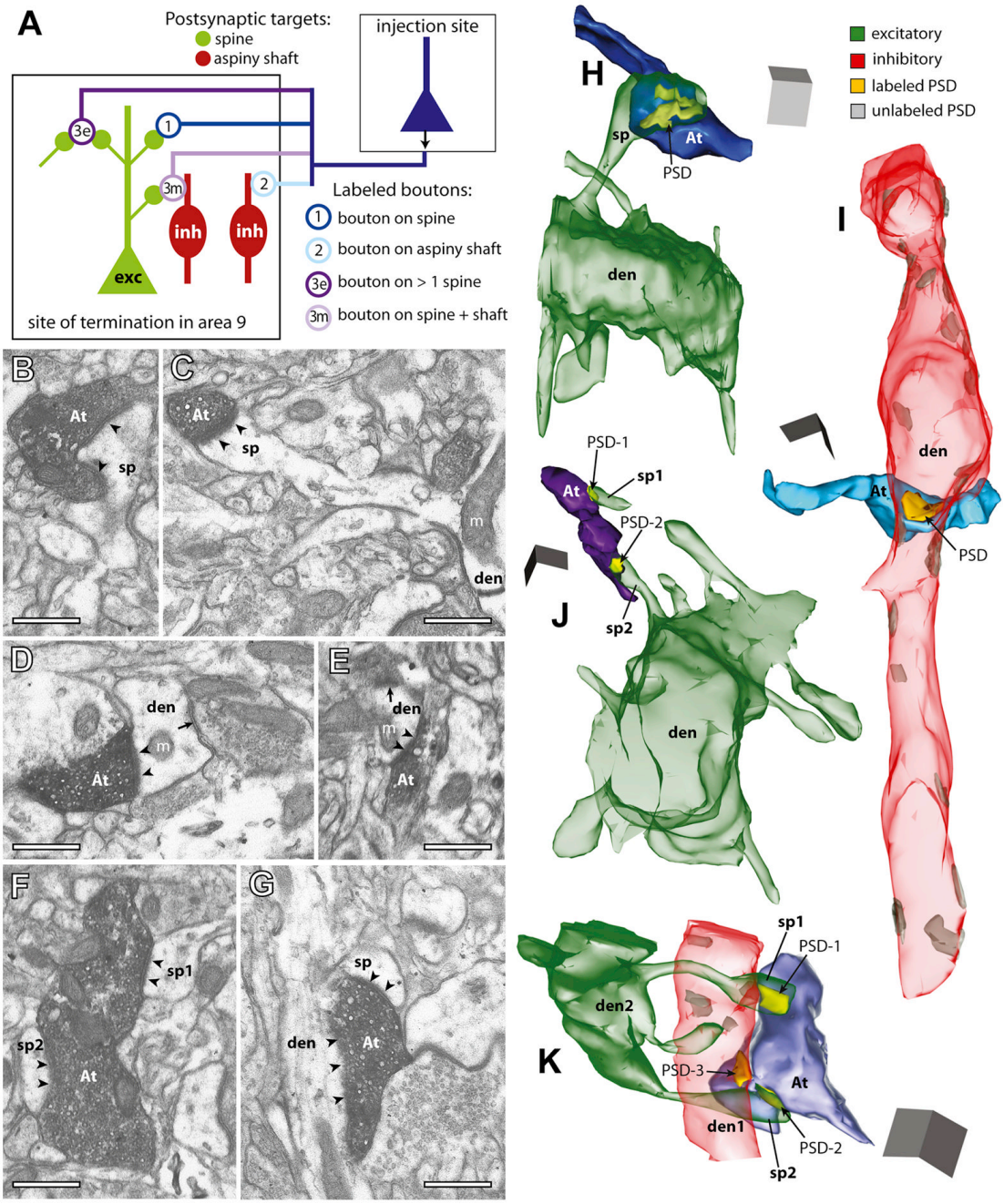

Figure 2. Postsynaptic targets of boutons from ACC (area 32) and area 46 in area 9

(A) Diagram shows the three main types of postsynaptic targets of labeled boutons (open circles) in area 9: (1) spines of excitatory (exc, green) neurons; (2) dendritic shafts of inhibitory (inh, red); or (3) multiple postsynaptic sites, involving more than one spine (3e, excitatory), or a spine and an aspiny shaft (3m, mixed).

(B–G) EM photomicrographs show examples of labeled axon terminals (At) and their synapses (arrowheads) with morphologically identified postsynaptic targets in 2D. **(B)** A bouton from area 32 and; **(C)** a bouton from area 46, each innervating a spine head (sp); the spine in C branches from a dendrite (den) with mitochondria (m). **(D)** A large bouton from area 32 and; **(E)** a small bouton from area 46, each innervating an aspiny shaft of an inhibitory neuron (den)

with a nearby shaft synapse (arrow) from an unlabeled terminal. **(F, G)** Large multisynaptic boutons from area 32: **(F)** one bouton forms synapses with two spines (sp1 and sp2) and; **(G)** another with a spine (sp) and an aspiny shaft (den).
(H–K) 3D reconstructions of labeled boutons and their postsynaptic densities (PSD) and targets in area 9: **(H)** A bouton from area 46 (At, dark blue) has a synapse (PSD, yellow) with a spine (sp, green translucent) branching from a spiny dendrite (den) of an excitatory neuron. **(I)** A bouton from area 32 (At, light blue) forms a synapse with an aspiny dendrite (den, red translucent) of an inhibitory neuron, which receives other shaft synapses (grey) from unlabeled terminals. **(J)** A bouton from area 46 (At, dark purple) forms synapses with two spines (sp1 and sp2); sp2 branches from a spiny dendrite (den). **(K)** A bouton from area 32 (At, light purple) forms synapses with an aspiny dendrite (den1) and two spines (sp1 and sp2) from the same spiny dendrite (den2). Scale bars = 0.5 μm.

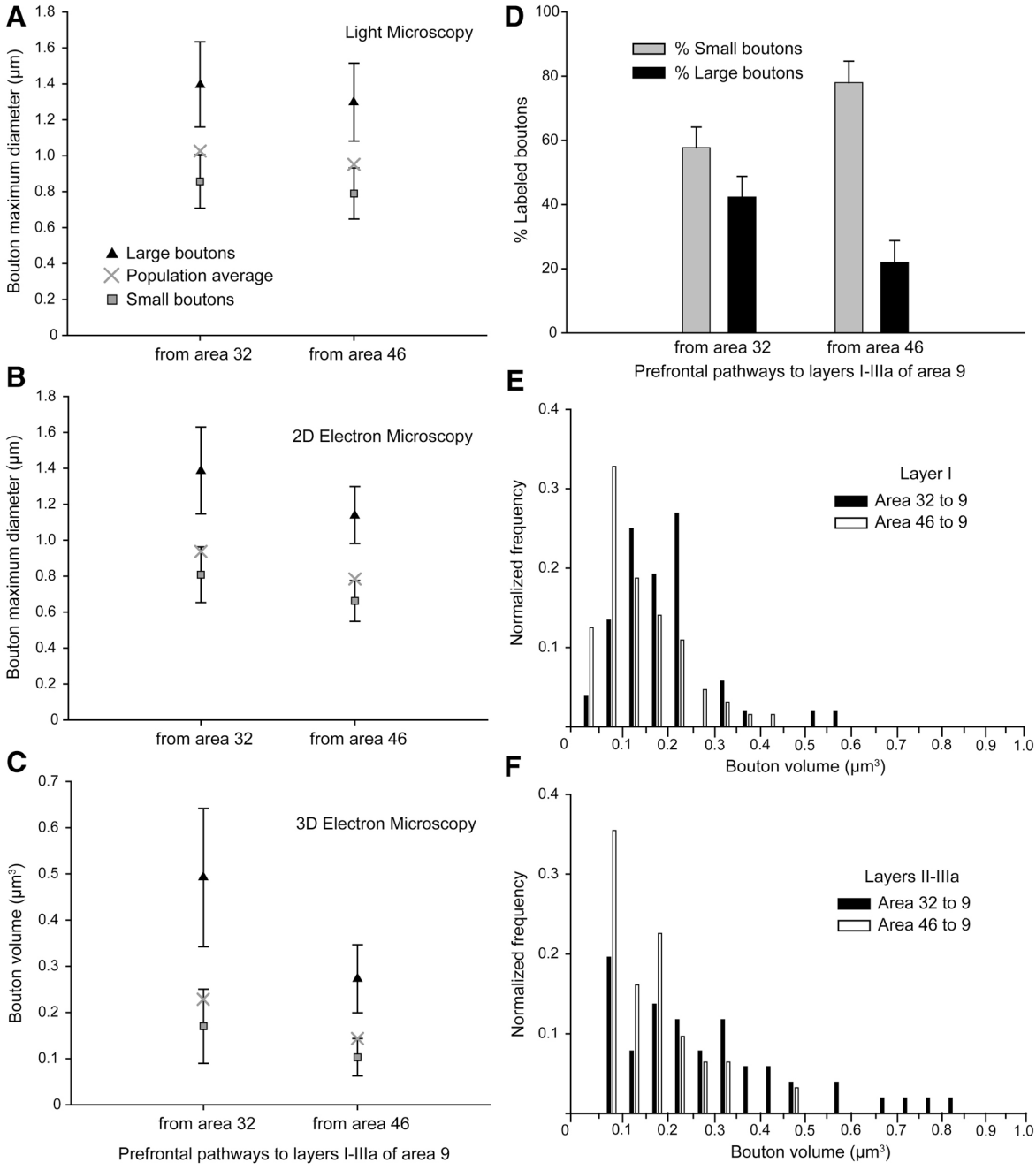

Figure 3. Bouton size differentiates pathways from ACC (area 32) and dorsolateral area 46 to area 9

(A–B) Average maximum major diameters and; **(C)** volumes of the total, large, and small labeled boutons in area 9 from areas 32 and 46, measured at the light microscope (A) and EM (B, C). Error bars = SD from cluster analysis.

(D) Proportion of small (grey) and large (black) labeled boutons from areas 32 and 46; data from EM and light microscopy were pooled. Error bars = SEM.

(E–F) Normalized frequency histogram of volumes of boutons from area 32 (black bars) and area 46 (silhouette bars) terminating in: **(E)** layer I and; **(F)** layers II-IIIa of area 9.

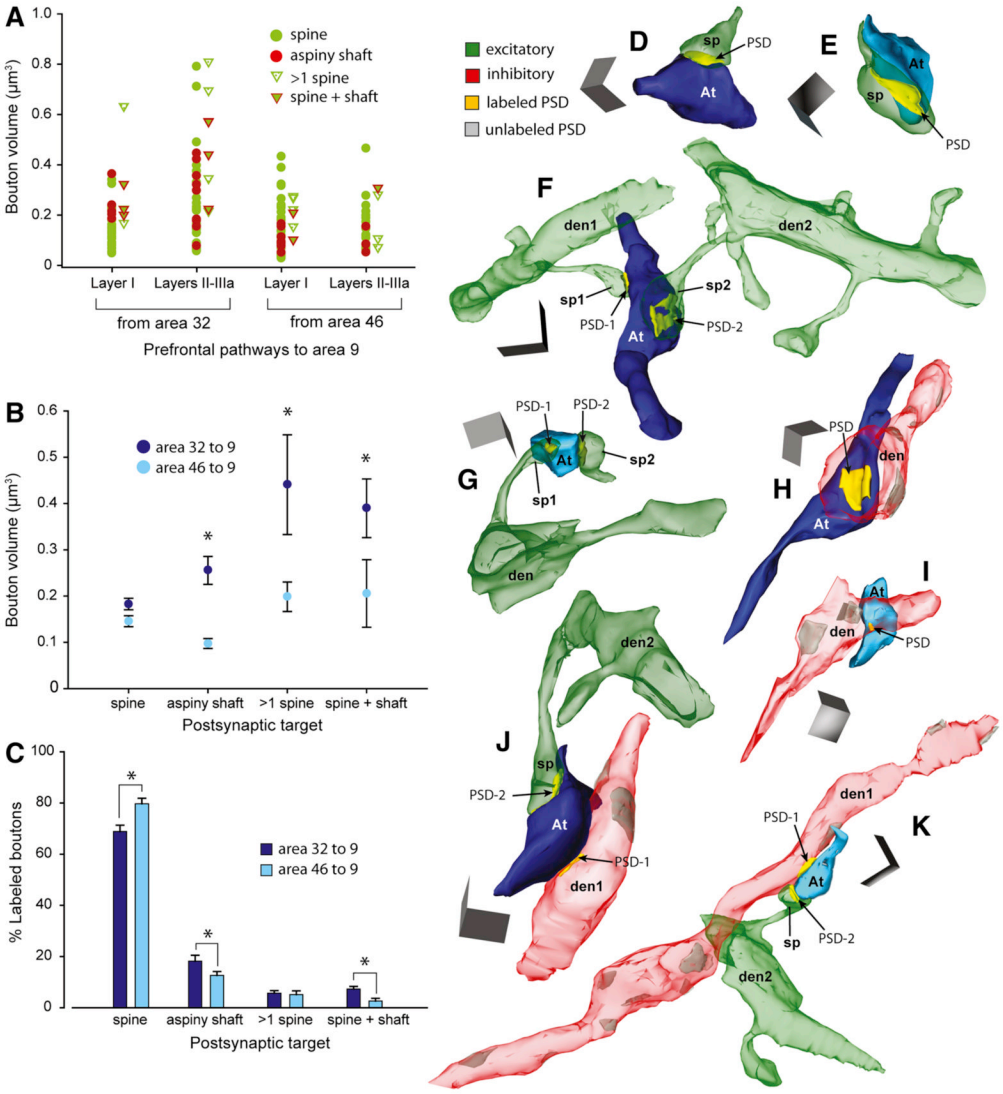

Figure 4. Presynaptic size differences correlate with type of postsynaptic target

(A) Scatter plot shows the volumes of individual boutons from area 32 (n = 91) and area 46 (n = 90) that formed synapses with distinct postsynaptic targets in layers I-IIIa of area 9.

(B) Average volume of boutons from area 32 (dark blue) and area 46 (light blue) with distinct postsynaptic targets. In the pathway from area 32, boutons were significantly larger than from area 46 when forming synapses with aspiny shafts of inhibitory neurons or with multiple postsynaptic sites ($p < 0.01$, asterisks), but not with synapses on single spines.

(C) Proportion of all labeled boutons with distinct postsynaptic targets. Boutons forming synapses with aspiny shafts, and spines and shafts were more prevalent from area 32 (on shafts, n = 67/345 boutons; spine + shaft, n = 23/345) than from area 46 (on shafts, n = 39/325; spine + shaft, n = 8/325); the opposite relationship was seen for boutons innervating spines (n = 235/345 from area 32; n = 261/325 from area 46). Statistically significant comparisons are marked with asterisks.

(D–K) 3D reconstructions of labeled boutons (At) in area 9 from area 32 (dark blue) and area 46 (light blue). **(D–E)** Small boutons that form a synapse (PSD, yellow) with a spine (sp, green) in layer I of area 9: **(D)** from area 32 and; **(E)** from area 46. **(F)** A large multisynaptic bouton from area 32 forms synapses with two spines (sp1 and sp2) in layers II-IIIa, branching from

dendrites (den1 and den2). **(G)** A small multisynaptic bouton from area 46 forms synapses with two spines (sp1 and sp2) in layers II-IIIa; sp1 branches from dendrite (den). **(H–I)** Boutons targeting aspiny dendrites of inhibitory neurons (den, red): **(H)** a large bouton from area 32 and; **(I)** a small bouton from area 46. **(J–K)** Multisynaptic boutons forming synapses with an aspiny shaft (den1) and a spine (sp) branching from a dendrite (den2): **(J)** a large bouton from area 32 and; **(K)** a small bouton from area 46. Scale bars = 0.5 μm. Error bars = SEM.

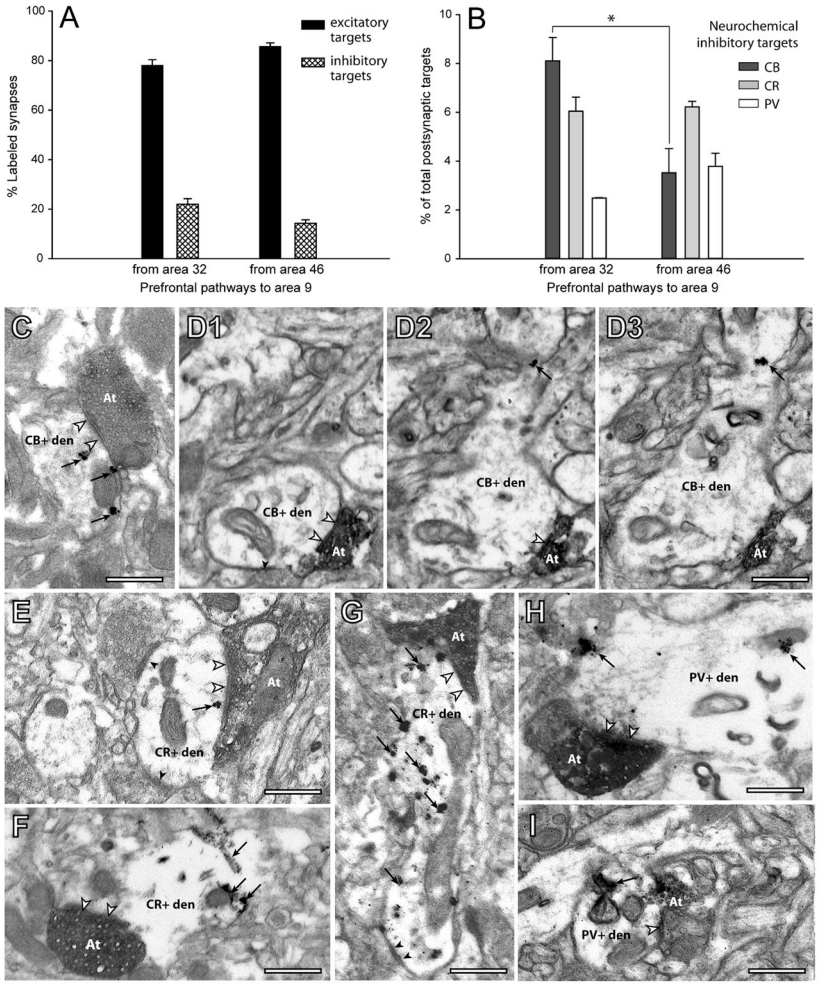

Figure 5. ACC area 32 and area 46 differentially innervate distinct neurochemical classes of inhibitory neurons in area 9

(A) Normalized distributions of all labeled synapses with spines (black) or with aspiny or sparsely spiny dendrites of inhibitory neurons (crosshatch) in area 9: axons from area 32 had more synapses on inhibitory neurons than area 46 ($p < 0.01$).

(B) Proportion of synapses with inhibitory neurons labeled with calbindin (CB), calretinin (CR), or parvalbumin (PV). ACC area 32 innervated significantly more CB neurons than area 46 ($p < 0.01$, asterisk).

(C–G) EM photomicrographs of labeled boutons (At) that form synapses (silhouette arrowheads) with distinct neurochemical classes of inhibitory neurons. **(C)** Large labeled bouton from area 32 (At) forms a synapse with a CB+ dendrite labeled with gold (arrows). **(D1–D3)** A series of three images of a small bouton from area 46 (At) that forms a synapse (arrowheads in D1 and D2) with a CB+ dendrite labeled with gold (arrows in D2 and D3). **(E–F)** Two large boutons (At) from area 32 form a synapse with a CR+ dendrite: one labeled with gold (E, arrow), another with TMB (F, arrows). The CR+ dendrite in E also receives synapses from two unlabeled boutons (black arrowheads). **(G)** A small bouton from area 46 (At) forms a synapse with a CR+ dendrite labeled with gold (arrows), which also receives a synapse from an unlabeled bouton (black arrowheads). **(H)** Large labeled bouton from area 32 (At) forms a synapse with a PV+ dendrite labeled with gold (arrows). **(I)** Small bouton from area 46 (At) forms a synapse with a PV+ dendrite labeled with TMB (arrow). Scale bars = 0.5 μm; Error bars = SEM.

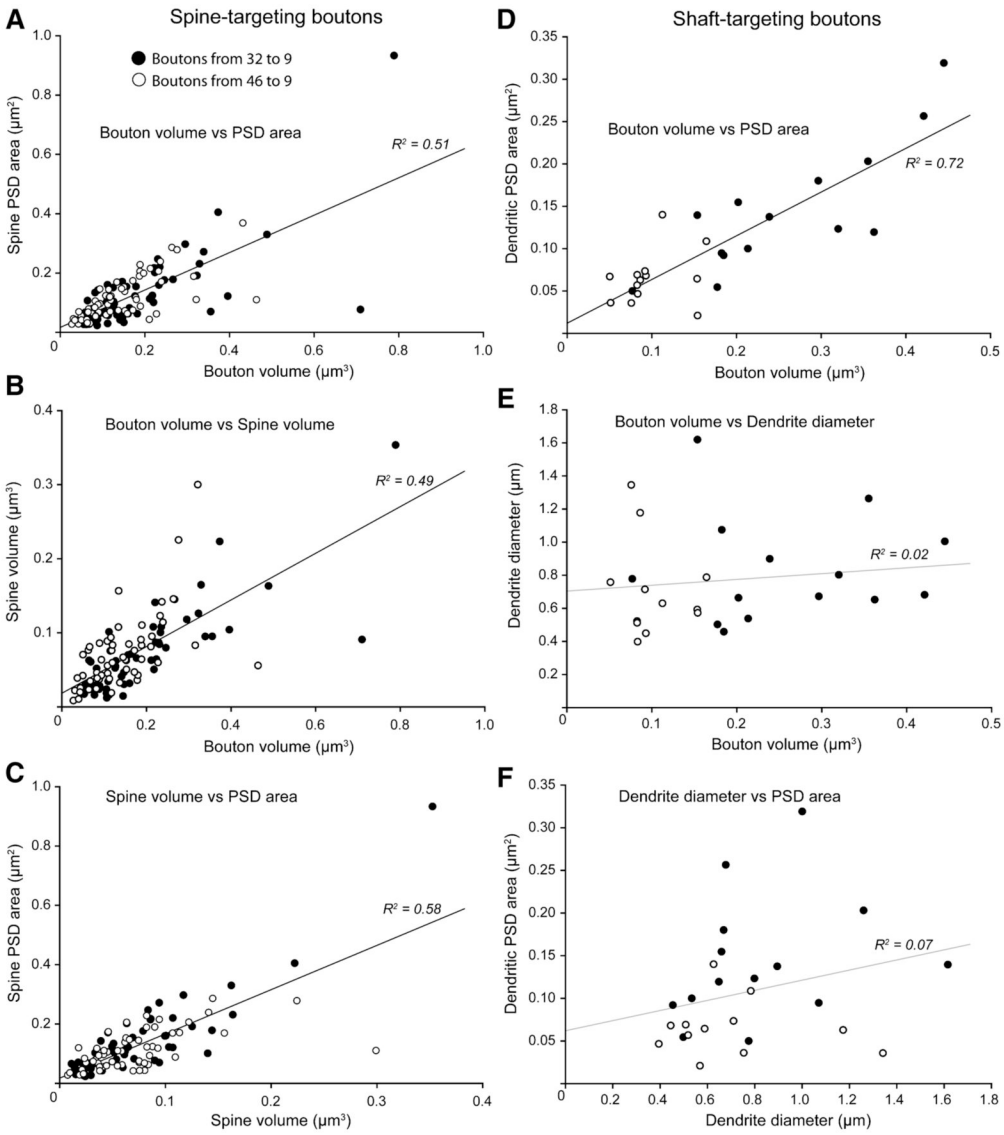

Figure 6. Relationship of presynaptic and postsynaptic features of prefrontal pathways

(A–C) Linear regressions for boutons targeting spines showing significant ($p < 0.01$) correlations of: **(A)** bouton volume and spine PSD area; **(B)** bouton volume and spine volume; **(C)** spine volume and PSD area.

(D–F) Linear regressions for boutons targeting dendritic shafts of inhibitory neurons. **(D)** Bouton volume and dendrite PSD area were significantly correlated ($p < 0.01$). **(E)** There was no correlation between bouton volume and dendrite diameter ($p = 0.53$), or; **(F)** between dendrite diameter and PSD area ($p = 0.21$).

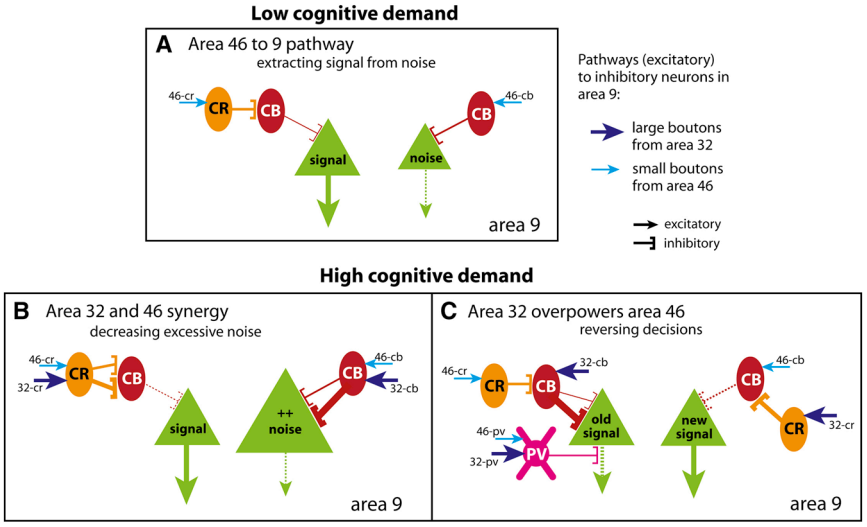

Figure 7. Summary of differential innervation of inhibitory neurons by distinct pathways and their possible role in cognitive control. Line thickness and size of arrows represent strength of connection (from data) or output. Dotted lines denote decrease in output

(A) Low cognitive demands in working memory: Activation of the pathway from area 46 to area 9 predominantly engages CR neurons (via 46-cr), which disinhibit pyramidal neurons. This pathway is consistent with disinhibiting activity in area 9 and enhancing relevant signals (large green triangle). Innervation of CB neurons is low, but a few may be activated (via 46-cb); this pathway is consistent with suppressing moderate noise (small green triangle).

(B) High cognitive demand: The pathways from area 46 and ACC (area 32) may act in synergy. When noise increases during high cognitive demands, suppression engaged by the area 46 pathway may not be enough. ACC may be recruited to suppress excessive noise by strongly activating CB neurons through efficient large boutons (via 32-cb). ACC may also engage CR neurons to further disinhibit the relevant signal drowned out by excessive noise (via 32-cr).

(C) High cognitive demand: Large ACC boutons may overpower the effects of small area 46 boutons to reverse decisions. CB inhibitory neurons activated by large boutons from ACC (32-cb) may overpower CR disinhibitory neurons engaged by small boutons from area 46 (46-cr) to suppress a previous signal (green, old signal). CR disinhibitory neurons may be recruited by large boutons from ACC (32-cr), overpowering CB neurons engaged by area 46 (46-cb) to enhance a new signal. In addition, the two pathways may recruit PV inhibitory neurons (46-pv and 32-pv), potentially shifting the temporal dynamics to reverse the response, with the large boutons from ACC acting as drivers (32-pv).